





Loss of Adenylyl Cyclase 6 in Leptin Receptor-Expressing Stromal Cells Attenuates Loading-Induced Endosteal Bone Formation

Mathieu Riffault,^{1,2,3†} Gillian P Johnson,^{1,2,3,4†} Madeline M Owen,^{1,2} Behzad Javaheri,⁵ 
Andrew A Pitsillides,⁵ and David A Hoey^{1,2,3,4} 

¹Trinity Centre for Biomedical Engineering, Trinity Biomedical Sciences Institute, Trinity College Dublin, Dublin, Ireland

²Department of Mechanical, Manufacturing, and Biomedical Engineering, School of Engineering, Trinity College Dublin, Dublin, Ireland

³Advanced Materials and Bioengineering Research Centre (AMBER), Royal College of Surgeons in Ireland and Trinity College Dublin, Dublin, Ireland

⁴Department of Mechanical, Aeronautical and Biomedical Engineering, University of Limerick, Limerick, Ireland

⁵Skeletal Biology Group, Comparative Biomedical Sciences, The Royal Veterinary College, London, United Kingdom

ABSTRACT

Bone marrow stromal/stem cells represent a quiescent cell population that replenish the osteoblast bone-forming cell pool with age and in response to injury, maintaining bone mass and repair. A potent mediator of stromal/stem cell differentiation in vitro and bone formation in vivo is physical loading, yet it still remains unclear whether loading-induced bone formation requires the osteogenic differentiation of these resident stromal/stem cells. Therefore, in this study, we utilized the leptin receptor (LepR) to identify and trace the contribution of bone marrow stromal cells to mechanoadaptation of bone in vivo. Twelve-week-old *Lepr-cre;tdTomato* mice were subjected to compressive tibia loading with an 11 N peak load for 40 cycles, every other day for 2 weeks. Histological analysis revealed that *Lepr-cre;tdTomato*⁺ cells arise perinatally around blood vessels and populate bone surfaces as lining cells or osteoblasts before a percentage undergo osteocytogenesis. *Lepr-cre;tdTomato*⁺ stromal cells within the marrow increase in abundance with age, but not following the application of tibial compressive loading. Mechanical loading induces an increase in bone mass and bone formation parameters, yet does not evoke an increase in *Lepr-cre;tdTomato*⁺ osteoblasts or osteocytes. To investigate whether adenylyl cyclase-6 (AC6) in LepR cells contributes to this mechanoadaptive response, *Lepr-cre;tdTomato* mice were further crossed with *AC6^{fl/fl}* mice to generate a LepR⁺ cell-specific knockout of AC6. These *Lepr-cre;tdTomato;AC6^{fl/fl}* animals have an attenuated response to compressive tibia loading, characterized by a deficient load-induced osteogenic response on the endosteal bone surface. This, therefore, shows that *Lepr-cre;tdTomato*⁺ cells contribute to short-term bone mechanoadaptation. © 2020 The Authors. *JBMR Plus* published by Wiley Periodicals LLC on behalf of American Society for Bone and Mineral Research.

KEY WORDS: ADENYLYL CYCLASE 6; BONE ADAPTATION; IN VIVO MECHANICAL LOADING; MECHANOBIOLOGY; STEM CELLS

Introduction

Physical loading is a potent regulator of bone anabolism, yet the cellular mechanisms by which this occurs are not fully understood.^(1,2) This mechanoadaptive response involves bone formation by osteoblasts which are derived from a progenitor or stromal cell population. The finite lifespan of the osteoblast suggests that these cells must be continuously replenished from a progenitor population to meet the cellular demand imposed by mechanical loading; a similar recruitment process operates in response to injury.^(3–7) Although load-induced stromal/stem

cell differentiation can be indirectly coordinated by the osteocyte,⁽⁸⁾ a recent study has shown loading-induced bone formation in a bone explant model that is independent of apparent mechanical stimulation of osteocytes.⁽⁹⁾ This indicates that applied mechanical stimulation may directly promote bone marrow stem/stromal cells (MSCs) osteogenesis.^(5,10) However, neither the load-induced MSC differentiation to osteoblasts nor the mechanistic basis for MSC mechanosensing has been fully elucidated in vivo.

The establishment of a robust MSC marker is critical for their identification and lineage tracing in vivo. MSCs are traditionally

This is an open access article under the terms of the Creative Commons Attribution License, which permits use, distribution and reproduction in any medium, provided the original work is properly cited.

Received in original form July 31, 2020; accepted August 27, 2020. Accepted manuscript online August 31, 2020.

Address correspondence to: David A Hoey, PhD, Mechanical & Manufacturing Engineering, Parsons Building, Trinity College Dublin, Dublin 2, Ireland.

E-mail: dahoe@tcd.ie

[†]MR and GPJ contributed equally to this work.

JBMR[®] Plus (WOA), Vol. 00, No. 00, Month 2020, e10408.

DOI: 10.1002/jbm4.10408

© 2020 The Authors. *JBMR Plus* published by Wiley Periodicals LLC on behalf of American Society for Bone and Mineral Research.

described as plastic-adherent, colony-forming, non-hematopoietic cells which can differentiate into chondrogenic, adipogenic and osteogenic progeny.^(3,11) Furthermore, MSCs are often perivascular in vivo, where murine MSCs are characterized by their lack of expression of hematopoietic (CD45) and endothelial markers (TER-119) and positive expression of platelet-derived growth factor receptor alpha (PDGFR α), stem cells antigen-1 (Sca1), CD51, CD105, CD90, nestin, α SMA, and combinations thereof.^(3,12–14) MSCs can therefore be retrospectively identified based on the above characteristics; yet an appropriate method for their prospective identification is lacking, and hence their location and physiological functions in vivo have remained elusive. Recently, leptin receptor-positive (LepR⁺) cells were identified as being perivascular and a major source of the stem cell fraction within the bone marrow.^(3,15–19) Additionally, these LepR⁺ cells were found to express the bone marrow MSC markers PDGFR α and CD51, and to be highly enriched for fibroblast colony-forming units. Moreover, analyses indicated that LepR⁺ cells in the bone marrow largely overlap with Nestin, an intermediate filament protein that is known as a neural stem/progenitor marker in adult bone marrow.^(3,20) LepR⁺ cells not only express MSC markers, but have now been shown to function as the main source of new osteoblasts and adipocytes in adult bone marrow and to be recruited to sites of injury to form bony ossicles that support hematopoiesis in vivo.⁽³⁾ Also, osteogenic differentiation of these cells is increased following anabolic stimulation with parathyroid hormone.⁽¹⁸⁾ Despite their presence in various tissues and organs^(21,22) and heterogenous nature,⁽¹⁹⁾ these characteristics suggest that LepR⁺ cells are a suitable candidate to determine the role of early progenitors in load-induced bone anabolic responses.

The candidature of these LepR⁺ cells as a means of prospectively identifying MSC fate is further supported by recent studies highlighting a role for the more committed osteoprogenitors in load-induced bone formation. Work by Liu and colleagues has focused on the effect of mechanical loading on primitive osteoprogenitors, looking specifically at Prrx1 (paired related homeobox 1) and Sca1-positive cells,⁽⁷⁾ and Zannit and Silva investigated the more committed osterix (Osx) positive osteoblast lineage cells.⁽²³⁾ Both report proliferation of these Prrx1⁺, Sca1⁺ and Osx⁺ cells following loading; however, the role of Prrx1 has been predominately characterized on the periosteum.

The osteogenic differentiation of MSCs can be directly driven by mechanical loading in vitro.^(10,24) Furthermore, we have previously shown that MSCs utilize adenylyl cyclases (ACs) to generate cAMP as a second messenger in this mechanotransduction leading to osteogenesis.⁽²⁵⁾ ACs are a family of transmembrane enzymes that catalyze the cyclization of adenosine triphosphate into cAMP.⁽²⁶⁾ The AC family comprises nine distinct transmembrane isoforms (AC1–AC9), each with individual regulatory properties and restricted expression in only a limited number of tissues.^(27,28) Specifically, AC6 has been shown to be expressed in skeletal cells and is required for load-induced bone formation in vivo.⁽²⁹⁾ Interestingly, skeletally mature mice, with a global deletion of AC6, did not present with a skeletal phenotype, but formed significantly less bone than control mice in response to ulna loading, showing that AC6 mediates bone mechanoadaptation.⁽²⁹⁾ Although this study clearly showed a role for AC6 in bone mechanobiology, given the global deletion of this enzyme, the specific cell type and mechanism of action of AC6 in bone mechanoadaptation remains unclear.

The development of the *Lepr-cre* mouse model along with specific deletion with Cre-lox recombination has provided a

means to study the fate of these cells and the role of associated molecules. Although LepR⁺ marrow stromal cells have been shown to be critical to adult bone formation, their role in mechanoadaptation is not known. Therefore, this study aimed to characterize the response of LepR⁺ marrow stromal cells to load-induced bone formation, and to explore whether these cells or their progeny contribute to load-related osteogenesis. Utilizing *Lepr-cre;tdTomato* mice, we have shown that LepR⁺ cells arise perinatally in bone, appearing perivascularly before expanding with age to undergo osteoblastic and osteocytic differentiation and act as the main source of bone-forming cells. We have shown that loading increases tibial bone formation and has little influence on the percentage of *Lepr-cre;tdTomato*⁺ stromal cells within the marrow. Moreover, no significant changes in the percentage of *Lepr-cre;tdTomato*⁺ cells lining bone surface or osteocytes were observed, suggesting that loading does not mediate the proliferation or recruitment of LepR⁺ cells. Furthermore, our data show that AC6 deletion in LepR⁺ cells restricts the endosteal cortical bone response to loading, highlighting the contribution of LepR⁺ cells and a critical role for AC6 in bone mechanoadaptation.

Materials and Methods

Mice

All transgenic mice were maintained in a C57BL/6 background. Transgenic mice B6.129-*Lepr*^{tm2(cre)Rck}/J JAX stock #008320,⁽²¹⁾ B6.Cg-Ct(ROSA)26Sor^{tm9(CAG-tdTomato)Hze}/J JAX stock #007909,⁽³⁰⁾ and B6;129-*Adcy6*^{tm1.1Dek}/J JAX stock #022503⁽³¹⁾ were purchased from the Jackson Laboratory (Bar Harbor, ME, USA), and rederived in-house. B6.129-*Lepr*^{tm2(cre)Rck}/J and B6.Cg-Ct(ROSA)26Sor^{tm9(CAG-tdTomato)Hze}/J were crossed to generate heterozygous B6.129-*Lepr*^{tm2(cre)Rck}/J and heterozygous B6.Cg-Ct(ROSA)26Sor^{tm9(CAG-tdTomato)Hze}/J breeding pairs. Female B6.129-*Lepr*^{tm2(cre)Rck}/J::B6.Cg-Ct(ROSA)26Sor^{tm9(CAG-tdTomato)Hze}/J offspring heterozygous for B6.Cg-Ct(ROSA)26Sor^{tm9(CAG-tdTomato)Hze}/J were used for all studies. This *Lepr-cre;tdTomato* mouse facilitates the labeling of cells actively expressing the leptin receptor, in addition to their progeny irrespective of receptor expression. Heterozygous *Lepr-cre;tdTomato* mice were subsequently crossed with B6;129-*Adcy6*^{tm1.1Dek}/J to generate animals with a knockout for AC6 in *Lepr-cre;tdTomato*-expressing cells resulting in a *Lepr-cre;tdTomato;AC6*^{f/f} mouse. Genotyping was achieved using DNA extracted from the ear and performed by Transnetyx (Memphis, TN, USA). All animals were maintained in groups of four under specific pathogen-free conditions at 24°C \pm 2°C with a 12-hour light/dark cycle and were provided with water and *ad libitum* diets. The procedures performed in this study were approved by Trinity College Dublin Animal Research Ethics Committee and Health Products Regulatory Authority in Ireland.

Histological analysis

Embryos, organs, and tibias from all groups were dissected, fixed for 12 hours in neutral buffered formalin (Sigma-Aldrich, St. Louis, MO, USA), decalcified in 10% EDTA (Sigma-Aldrich), and processed for standard paraffin embedding. Transverse 10- μ m sections were taken from individual samples and two sections were used in subsequent procedures. Prior to staining, sections were dewaxed and rehydrated. For hematoxylin and eosin (H&E) staining, sections were stained with HARRIS hematoxylin

solution (Sigma-Aldrich) for 4 min before rinsing and staining with eosin Y solution (Sigma-Aldrich) for 2 min. Sections were subsequently rehydrated and mounted using Distyrene Plasticizer Xylene (DPX) (Sigma-Aldrich). Slides were imaged on an Aperio Scanscope CS2 (Leica Biosystems, Wetzlar, Germany). For immunofluorescence studies, bone tissue was fixed, decalcified, and cryo-embedded. Sections of 20 μm were sliced with a cryostat. Then 4,6-diamidino-2-phenylindole (DAPI) at 1:2000 in PBS (Sigma-Aldrich) was applied to all samples for 5 min prior to sample-mounting on glass slides using ProLong Gold mounting medium (Invitrogen, Carlsbad, CA, USA). Leptin receptor staining was performed after antigen retrieval with proteinase K solution (20 min at 37°C) in a humidified chamber. Slides were then washed with PBS-Tween 0.5% v/v and blocked (5% BSA in PBS, 1 hour at 37°C). Slides were incubated in the primary antibody against leptin receptor (1:200; AF497; R&D Systems, Minneapolis, MN, USA), washed, and then further incubated in secondary antibody (1:500; Ab150129; Thermo Fisher Scientific, Waltham, MA, USA). DAPI at 1:2000 in PBS was then applied before mounting using ProLong Gold mounting medium. Imaging was performed on the Leica SP7 (Leica Microsystems, Wetzlar, Germany) scanning confocal microscope at $\times 20$.

Flow cytometry

To quantify the percentage of Tomato⁺ cells in a given population, organs were harvested, minced, and homogenized, and cell suspension filtered through a 70- μm cell strainer. After centrifugation, cell pellets were resuspended in red blood cell lysis buffer (20mM of Tris, 150mM of NH₄Cl in diH₂O), for 5 min on ice, then washed and resuspended in 1-mL flow cytometry buffer composed of PBS (Sigma-Aldrich) with 0.5% BSA (Sigma-Aldrich) and 2mM EDTA (Sigma-Aldrich, pH 7.2).

Left and right tibias were isolated, and the bone marrow was flushed from the marrow cavity with 3-mL DMEM (Sigma-Aldrich). Once flushed, cells were centrifuged at 400g for 5 min and resuspended in 1-mL red blood cell lysis buffer for 5 min on ice. Cells were washed before subsequent re-suspension in 2% PBS- FBS and incubated on ice for 30 min. Cells were then incubated for 30 min on ice with CD45 (CD45-BV421, 563890; 1:100; BD Biosciences, San Jose, CA, USA) and TER-119 (TER-119-BB515, 564760; 1:100; BD Biosciences) antibodies. After washing in PBS, cells were resuspended in 1-mL flow cytometry buffer. Flow cytometry analysis was performed on a BD LSRFortessa (BD Biosciences) at medium speed and gated at 100,000 events of Tomato⁺ cells.

In vivo axial tibia loading

Mice at 12 weeks of age were initially anesthetized using 4% isoflurane and then maintained at 1.5% to 2% isoflurane during the remainder of the procedure. The right tibia was placed between two cups attached to an electromagnetic loading system with feedback control (ElectroForce 5500; TA Instruments, New Castle, DE, USA). After an initial 2-N load, a peak compressive load of 11 N was applied, for 40 cycles with 10 s of rest between each cycle every second day for 2 weeks as previously described.⁽³²⁾ Left tibias served as nonloaded internal controls. Body weight was measured at 12 weeks of age and on subsequent loading days. All animals were euthanized on day 18 and prepared for either dynamic histomorphometric, histological, or flow cytometry analysis.

Microcomputed tomography analysis

Mice were placed under isoflurane-induced anesthesia as described above. Tibias were imaged by in vivo μCT (Scanco VivaCT 80; Scanco Medical AG, Brüttisellen, Switzerland). The cortical area was scanned with a voxel size of 25 μm . Scans were performed using a voltage of 70 kVp, a current of 114 μA and a 200-ms integration time. A Gaussian filter ($\sigma = 0.8$, support = 1) was used to suppress noise and a global threshold of 150 was applied for analysis of cortical bone scans. The bone volume, cortical area and thickness, second moment of area around major/minor (I_{min} and I_{max}) were quantified using scripts provided by Scanco.

Whole-body scans were taken for phenotypic analysis of *Lepr^{cre};tdTomato;AC6^{fl/fl}* mice. Briefly, after euthanasia, whole-body scans were performed at 15- μm voxel size. Scans were performed using a voltage of 70 kVp, a current of 114 μA , and a 200-ms integration time. A Gaussian filter ($\sigma = 0.8$, support = 1) was used to suppress noise and a global threshold of 150 was applied to generate the 3D reconstruction using scripts provided by Scanco.

Whole-bone analysis was performed on data sets derived from CT scans using BoneJ⁽³³⁾ (version 1.4.2), an ImageJ plugin (NIH, Bethesda, MD, USA; <https://imagej.nih.gov/ij/>). Following segmentation and removal of fibula from the data set, a minimum bone threshold was selected using a histogram-based method in ImageJ that utilizes all pixels in a stack to construct a histogram and was further confirmed using ImageJ Threshold function. A threshold of 100 was applied to all data sets to separate higher density bone from soft tissues and air. This threshold was used in Slice Geometry function within BoneJ to calculate bone cross-sectional area, second moment of area around the minor axis (I_{min}), second moment of area around the major axis (I_{max}), mean thickness determined by local thickness in two dimensions (cortical thickness), ellipticity and predicted resistance to torsion (J). The most proximal (0%–15%) and the most distal portions (85%–100%) of tibial length were excluded from analysis, as these regions include trabecular bone.

Dynamic histomorphometry

Mice were injected with calcein (15 mg/kg body weight; Sigma-Aldrich) on the third and sixth day of loading. Left and right tibias were isolated, cleaned of soft tissue, fixed in formalin (Sigma-Aldrich), and stored in 70% ethanol for dynamic histomorphometry. The tibias were dehydrated in graded alcohol (70%–100%), infiltrated with three changes of Technovit 9100 methyl methacrylate (C N Technical Services Ltd, Wisbech, England), and embedded in Technovit 9100 following the manufacturer's recommendation. Transverse sections of the embedded tibia midshaft were imaged on a Leica SP7 (Leica Microsystems) scanning confocal microscope. Measurements of the bone perimeter, single-label perimeter, double-label perimeter, and double-label area were completed with Fiji⁽³⁴⁾ (version 1.6.0_24) and used to calculate mineralizing surface/bone surface, mineral apposition rate (MAR), and bone formation rate (BFR)/bone surface. Measurements were taken at both the endosteum and periosteum.

Immunofluorescence image analysis

A ROI for cortical bone spanning 100 slices (2500 μm) was selected 3 mm from the tibia–fibula junction towards the tibial proximal metaphysis. Using Fiji, the length of the bone surface covered by Tomato⁺ cells at both endosteal and periosteal

surfaces, and the number of Tomato⁺ cells embedded within bone were counted within the ROI.

To determine if endosteal regions showing bone formation by dynamic histomorphometry correlate with regions where Tomato⁺ cells are observed on confocal images, both sets of images were analyzed with Fiji. To compare between different animals, the total length of the endosteum was measured and expressed in percentage (0% starting at the tibial ridge, going clockwise to 100%). Locations, where one or two labels of calcein are observed, were determined and plotted against the total length of the endosteum for static and loaded bones. Then, the presence of tdTomato⁺ cells along the endosteum was observed and plotted against the total length of the endosteum. Results were averaged and pooled in clusters of 5%.

Statistical analysis

For flow cytometry of different tissues, a one-way ANOVA analysis was performed with Tukey correction. Dynamic histomorphometry analysis of *Lepr-cre;tdTomato;ACG^{fl/fl}* and comparison with WT mice was performed with a two-way ANOVA with Tukey correction. For all other studies, unpaired two-tailed student *t* test with Wilcoxon correction was employed. Data were analyzed using Graph Pad Prism 8 (GraphPad Software, Inc., La Jolla, CA, USA); for gross cortical bone morphology analysis, graphs were plotted using programming language R, version 3.1.3 (R Foundation for Statistical Computing, Vienna, Austria; <http://www.r-project.org>). The number of animals is detailed in the captions for each figure. In all experiments, *p* < 0.05 was considered statistically significant.

Results

LepR⁺ bone marrow cells are the main source of bone-forming cells

LepR⁺ bone marrow cells are the main source of bone forming cells on the early endosteal surface and later periosteal surface in addition to embedded osteocytes. We first analyzed the spatiotemporal expression of LepR⁺ cells in our model. Tomato⁺ cells were identified prenatally at E19.5 in the brain and ossification zone of the radius, ulna, and tibia (Fig. S1). The pattern of Tomato⁺ cells was further investigated in all major organs postnatally (Fig. S2). H&E staining was used to investigate the anatomy of organs and to more accurately identify the location of Tomato⁺ cells at 8 and 12 weeks of age (Fig. S2A–F). Tomato⁺ cells were found in various organs including the liver, kidney medulla, lung, spleen, and heart (Fig. S2A,B, D–F). Tomato⁺ cells increased with age, from 8 to 12 weeks, in each of these organs. Quantification of cell number within each organ of the *Lepr-cre;tdTomato* mouse was performed using flow cytometry at 12 weeks, which further highlighted the spatial differences in Tomato⁺ cells. At 12 weeks of age, Tomato⁺ cells accounted for <7% of cells in each organ, with the exception of the liver where 38% of cells were Tomato⁺.

The expression of *Lepr-cre;tdTomato*⁺ cells in 8- and 12-week-old mice was analyzed in greater detail within the tibia. Sagittal sections of the tibia were imaged using confocal microscopy and the trabecular and cortical bone regions examined for patterns of Tomato⁺ cell expression (Fig. 1). First, investigation of the trabecular region of the tibia of 8-week-old *Lepr-cre;*

tdTomato mice, revealed the presence of Tomato⁺ cells within the marrow space between trabeculae (Fig. 1Bi,Cii) where these cells located around sinusoids (Fig. 1Bii). Small populations of Tomato⁺ cells were also found lining and embedded within trabecular struts (Fig. 1Bi,Ci,Dii). Although Tomato⁺ cells are located perivascularly and along the bone surface, no Tomato⁺ cells were found in the growth plate (Fig. 1Di). By 12 weeks of age, the prevalence of Tomato⁺ cells located perivascularly within the trabecular bone marrow increased (Fig. 1Ei,Eii), whereas Tomato⁺ cells also increased along and within the trabecular bone. Interestingly, at 12 weeks of age, these cells along the surface of trabecular bone morphologically resembled that of osteoblasts (cuboidal) and bone-lining cells (flattened) (Fig. 1F, yellow arrows) suggestive of osteoblastic differentiation of LepR⁺ bone marrow stromal cells. Furthermore, the population of Tomato⁺ cells embedded within the trabecular bone (Fig. 1F, green arrows) is evidence of osteocytic differentiation.

Examining the cortical bone region of the tibial mid-diaphysis, a small population of Tomato⁺ cells were found perivascularly within the marrow and along the bone surface at 8 weeks of age (Fig. 2A). The pattern of expansion of this cell population seen in trabecular bone also held true when the cortical bone was further examined (Fig. 2B–D); at 12 weeks, Tomato⁺ cells are found perivascularly, along the endosteal surface (Fig. 2Cii and D, yellow arrow) and embedded within the cortical bone (Fig. 2D, green arrows). This observation was confirmed using flow cytometry, which showed that the percentage of Tomato⁺ cells in the marrow is $3.41 \pm 2.50\%$ in the tibia and $3.02 \pm 1.98\%$ in the femur in 12-week-old mice (Fig. 2E). Furthermore, LepR⁺CD45⁺Ter119⁺ bone marrow stromal cells accounted for $0.16 \pm 0.11\%$ of bone marrow cells within the tibia (Fig. 2F). Together, these data suggest that *Lepr-cre;tdTomato*⁺ bone marrow stromal cells appear perivascularly, where they expand with age, are recruited to the bone surface of both trabecular and cortical bone, and undergo osteoblastic and osteocytic differentiation.

Tibial loading enhances endosteal and periosteal cortical bone formation

To investigate whether there are changes in the LepR⁺ stromal cell pool and their progeny during loading-induced bone formation, a compressive load of 11 N was applied to the tibia of 12-week-old female *Lepr-cre;tdTomato* mice (Fig. 3A–C). Consistent with previous studies, our data show that tibia loading in this model leads to an anabolic response in cortical bone of *Lepr-cre;tdTomato* mice (Fig. 3D–F). Analysis of the entire tibial cortex by μ CT reveals an increase in cross-sectional area following loading, as well as a greater cross-sectional ellipticity (Fig. 3D). The second moment of inertia around the major (I_{\min}) and minor (I_{\max}) axes and the predicted resistance to torsion (*J*) are also enhanced following the 2 weeks of loading in *Lepr-cre;tdTomato* mice (Fig. S4).

Bone formation was also measured on both the endosteal and periosteal surfaces using dynamic histomorphometry, where right (loaded) tibias formed significantly more bone than left (nonloaded) tibias (Fig. 3E,F). After 2 weeks of loading, we found a significant increase in mineralized surface, MAR, and BFR at both the endosteal (Fig. 3E) and periosteal surfaces (Fig. 3F). Mineralized surface, MAR, and BFR were increased by 30%, 20%, and 79% on the endosteal surface, respectively (Fig. 3E), whereas on the periosteal surface mineralized surface,

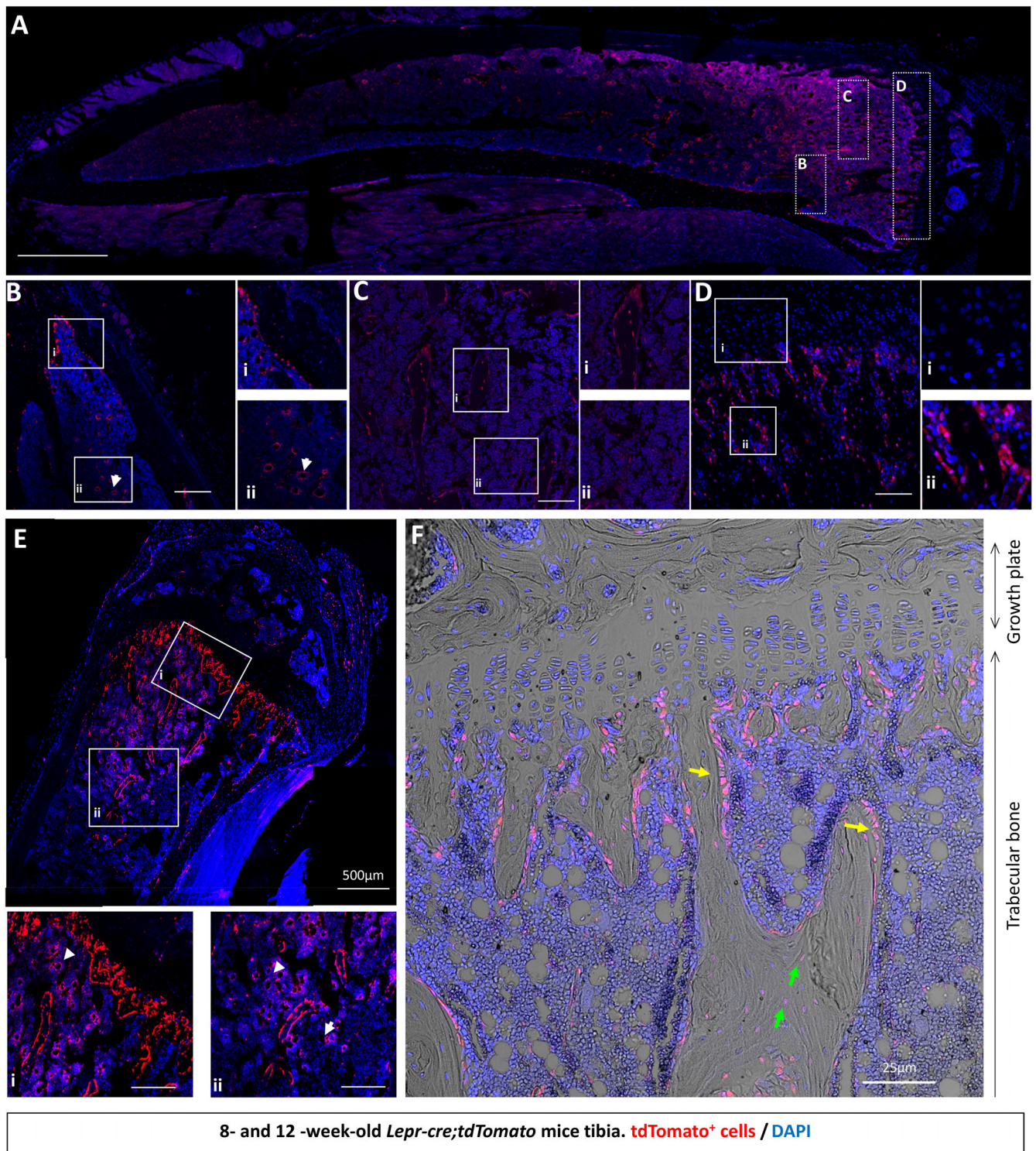


Fig 1. tdTomato⁺ bone marrow cells appear around sinusoids and contribute to osteoblast and osteocyte populations over time in trabecular bone. To assess whether *Lepr-cre* was actively expressed in adult tibia, limbs were harvested from 8- and 12-week-old *Lepr-cre;tdTomato* mice and processed for histological analyses with the nuclear dye 4,6-diamidino-2-phenylindole (DAPI). (A) Representative image of an 8-week-old tibia, showing ROIs. (B–D) Confocal microscopy revealed tdTomato⁺ signal in 8-week-old trabecular bone marrow (B–Bi), perivascularly in the marrow space (arrow head; Bii), in trabecular bone (C), and below the growth plate (D). (Di) No staining was found in the growth plate. (E–F) Confocal microscopy revealed tdTomato⁺ signal in 12-week-old mice along the trabecular bone (E) and in trabecular bone marrow (Ei,ii). (Ei,ii) tdTomato⁺ was found to be perivascular in the marrow space (arrow head). (F) No staining was found in the growth plate. Additionally, tdTomato⁺ is expressed on the bone surface (yellow arrow) and embedded within bone (green arrow) in 12-week-old mice. *N* = 4. Scale bar = 50 µm unless otherwise indicated.

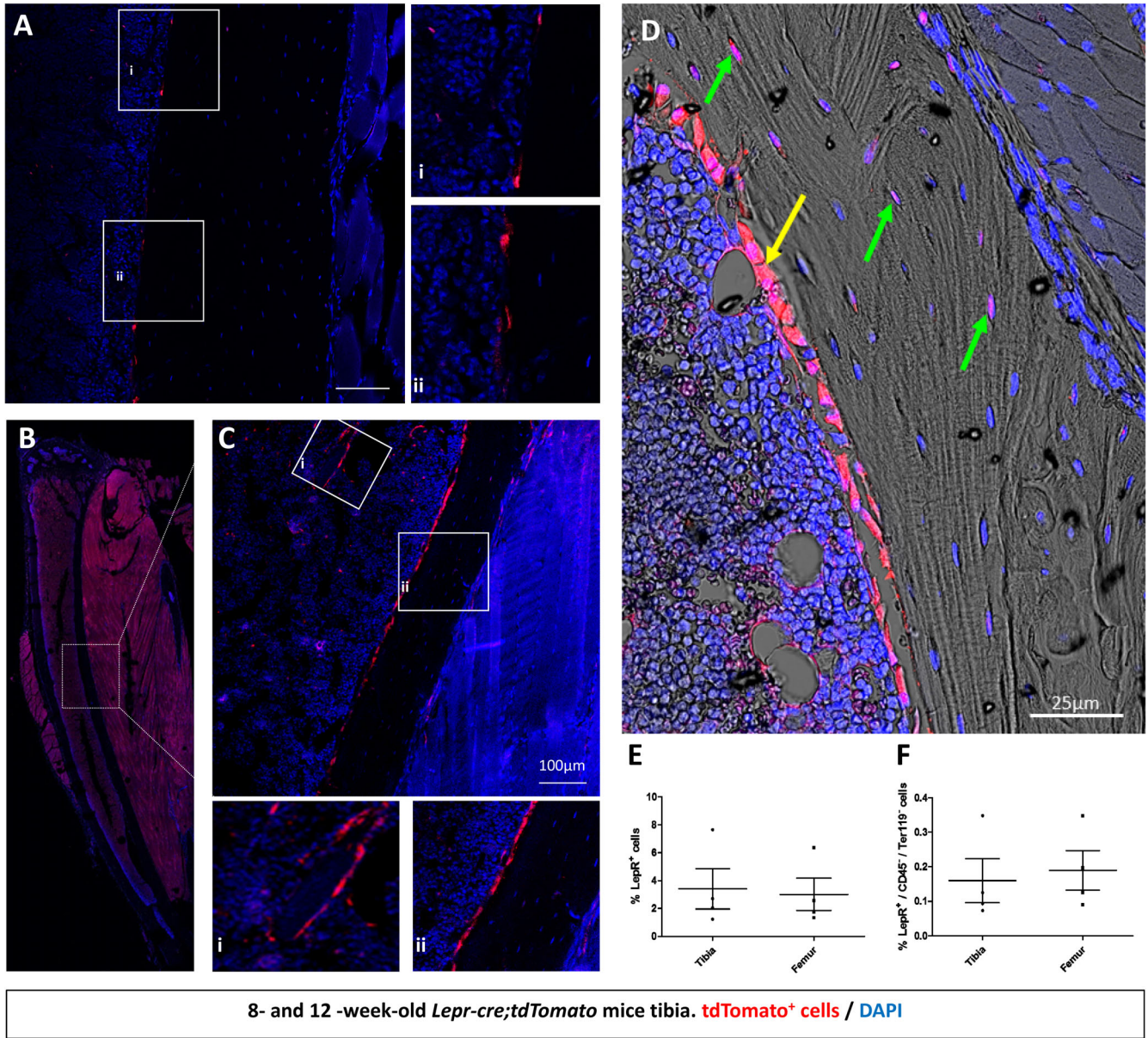


Fig 2. tdTomato⁺ bone marrow cells appear around sinusoids and contribute to osteoblast and osteocyte populations over time in cortical bone. To assess whether *Lepr-cre* was actively expressed in adult tibia, limbs were harvested from 8- and 12-week-old mice. *Lepr-cre;tdTomato* mice were processed for histological analyses with the nuclear dye 4,6-diamidino-2-phenylindole (DAPI). (A) tdTomato⁺ signal was found on the endosteal surface of cortical bone at 8 weeks. (B–D) Representative image of a 12-week-old tibia. (C_i,ii) confocal microscopy revealed LepR signal perivascularly in the marrow space (C_i) and along the cortical bone surface (C_{ii}). (D) LepR is expressed on the bone surface (yellow arrow) and embedded within bone (green arrow). *N* = 4. Scale bar = 50 μm. (E) Flow cytometry analyses revealed that in 12-week-old mice tdTomato⁺ make-up 1.23% to 7.65% and 1.35% to 6.36% of bone marrow cells in the tibia and femur, respectively. (F) Exclusion of CD45/Ter119⁺ cells reveals 0.07% to 0.35% and 0.09% to 0.34% tdTomato⁺ cells in the tibia and femur, respectively. *N* = 3. Values are percentages ±SD.

MAR, and BFR increased by 23%, 10%, and 28%, respectively (Fig. 3F).

Tibial loading does not influence the number of LepR⁺ bone marrow stromal cells or their progeny

To determine whether these load-related increases in cortical bone formation are linked to an expansion and differentiation of the *Lepr-cre;tdTomato*⁺ marrow stromal cell population, bone

marrow was flushed from the loaded and nonloaded tibias, and flow cytometry was performed to assess the percentage of Tomato⁺ cells. The percentage of Tomato⁺ cells did not increase following tibia loading when no cellular subgroups were excluded (Fig. 4A). However, when the CD45⁺ hematopoietic and TER-119⁺ erythropoietic cells were excluded, the percentage of Tomato⁺ stromal cells was found to be slightly greater (Fig. 4B). Although not significant, this could be indicative of a proliferative response in these primitive Tomato⁺ cells. Interestingly, additional staining

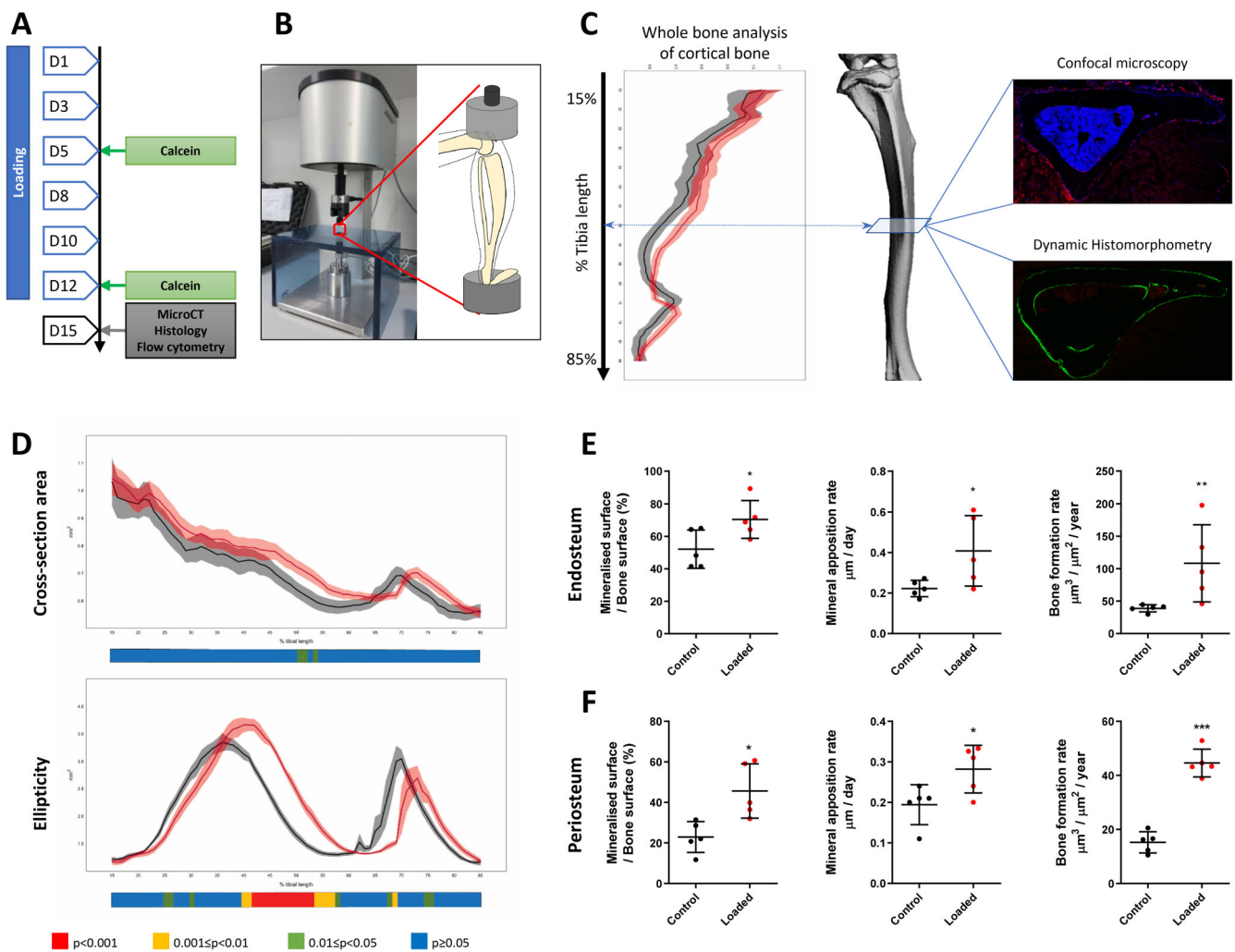


Fig 3. Axial tibia loading of 12-week-old *Lepr-cre;tdTomato* mice. (A) Schematic of the experimental plan and tibia loading setup. (B) The right tibia of 12-week-old mice was axially loaded at 11 N for 40 cycles with 10-second rest periods per day for 14 days. The left tibias were not loaded and were used as nonloaded internal controls. (C) Schematic representation of analyses done on tibias. Whole-bone μ CT was performed and cortical bone analyzed between 15% and 90% of the total tibial length. Confocal microscopy of cryosections and dynamic histomorphometry were performed on cross-sections located between 45% and 50% of the tibial length. (D) Whole-bone analyses of cortical bone between 15% and 85% of the total tibial length, excluding proximal and distal metaphyseal bone, showing cross-sectional area and ellipticity. Loaded: red, static: black, line graphs represent means \pm SEM, $n = 7$. Statistical significance of differences along the entire tibial shaft is represented as a heat map, red $p < 0.001$, yellow $0.001 \leq p < 0.01$, green $0.01 \leq p < 0.05$, and blue $p \geq 0.05$. (E–F) Dynamic histomorphometry analysis of tibial transverse section reveals tibial compressive loading enhances endosteal and periosteal cortical bone formation. Relative mineralizing surface over bone surface, mineral apposition rate, and bone formation rate at the endosteal (E) and periosteal (F) surface of mechanically loaded tibia. $N = 5$. Mean \pm SD.

of LepR (Fig. S3) reveals a colocalization of the signals from tdTomato⁺ and LepR antibody only in the marrow; Tomato⁺ cells lining bone surfaces and Tomato⁺ osteocytes do not show immunolabeling for LepR, indicating that they are not actively expressing LepR at the time of tissue collection on day 17.

The effect of loading on the numbers of Tomato⁺ cells, either lining or embedded within bone, which originated from LepR⁺ stromal cells was further assessed using histology (Fig. 4C). No change in the percentage of Tomato⁺ cells lining the endosteal or periosteal surface or in the cells embedded in the bone as osteocytes was observed in response to tibial loading (Fig. 4D).

The location of Tomato⁺ cells lining the endosteal surface was further analyzed and compared with the location where active bone formation had been detected by dynamic histomorphometry (Fig. 4E). This revealed that areas of endosteal surface where active bone formation ranged from 25% to 45%, 55% to 70%, and 80% to 95% (Fig. 4E, upper graph) failed to exhibit any correlative difference in the local number of Tomato⁺ cells (Fig. 4E, lower graph).

These data indicate that our loading protocol, which increases bone formation, does not significantly induce proliferation of LepR⁺ bone marrow stromal cells. Moreover, there is no recruitment of this cell type to the bone surface, suggesting that a

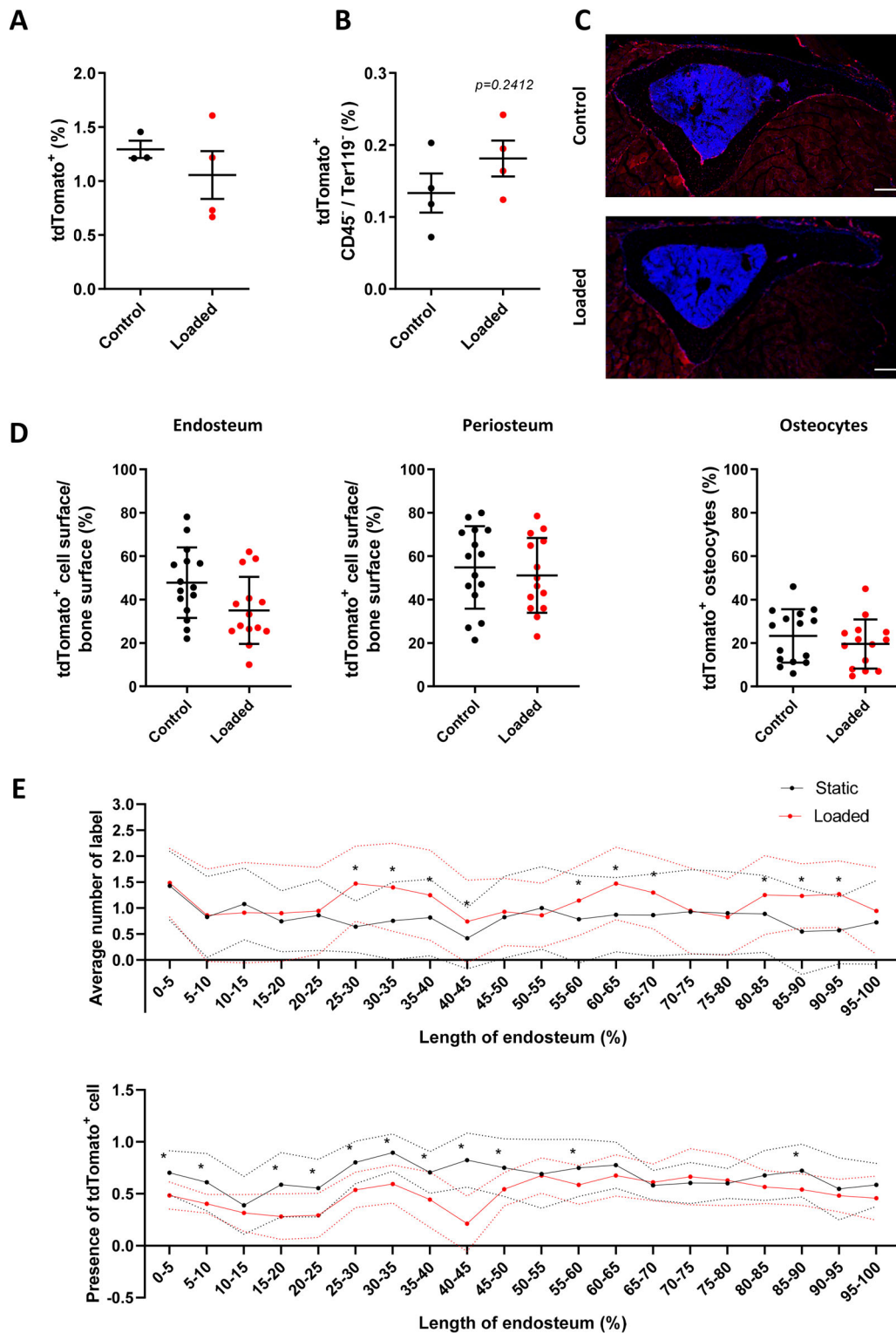


Fig 4. Tibial compressive loading does not alter proliferation or location of *Lepr-cre;tdTomato* cells. (A–B) Flow cytometry analyses of bone marrow cells following mechanical loading of *Lepr-cre;tdTomato* mouse tibia. (A) Flow cytometry analyses revealed loading did not alter the percentage of tdTomato⁺ cells. (B) Exclusion of CD45⁺ and Ter119⁺ cells reveals a trend towards an increase in tdTomato⁺ cells following tibia loading; $n = 4$. (C,D) Tibial compressive loading does not alter the location of tdTomato⁺ cells. (C) Representative image of tibia transection; scale bar = 100 μ m. (D) The percentage of tdTomato⁺ cells on the endosteal or periosteal surface and embedded with the bone was not altered in cortical bone following tibia compressive loading; $N = 7$. (E) Analysis of the location of bone formation along the surface of the endosteum. Upper graph: Average number of label observed by dynamic histomorphometry; $n = 4$. Lower graph: Average number of tdTomato⁺ cells observed lining endosteum surface on confocal images; $n = 3$. Statistical tests employed unpaired two-tailed student *t* test. Mean \pm SD; * $p < 0.05$.

reactivation of the cells already present at this location is responsible for the increased load-related bone accrual response.

LepR⁺ cells play a role in loading-induced bone formation via an AC6-dependent mechanism

To investigate whether cells derived from LepR⁺ stromal cells play a role in load-induced bone formation, we crossed the *Lepr-cre;tdTomato* mouse with the AC6 floxed animal *AC6^{fl/fl}* to generate an AC6 knockout in leptin receptor-expressing cells and their progeny (*Lepr-cre;tdTomato;AC6^{fl/fl}*). Utilizing a global deletion of AC6, it has been previously shown that AC6 is required for loading-induced bone formation.⁽²⁹⁾ However, it is unclear in which cell type AC6 is mediating this response. *Lepr-cre;tdTomato;AC6^{fl/fl}* mice were healthy and fertile, and appeared phenotypically normal (Fig. 5A,B, Fig. S5). Body weight of all mice

in the study increased with age, with no differences observed between *Lepr-cre;tdTomato* control animals and *Lepr-cre;tdTomato;AC6^{fl/fl}* mice at any time point (Fig. S5A). On average, the body weights of *Lepr-cre;tdTomato* and *Lepr-cre;tdTomato;AC6^{fl/fl}* mice were not significantly different at 8 or 12 weeks of age: *Lepr-cre;tdTomato* mice weighed 17.0 ± 0.1 g and 18.9 ± 0.4 g at 8 and 12 weeks, respectively, whereas *Lepr-cre;tdTomato;AC6^{fl/fl}* mice weighed 17.7 ± 0.4 g and 19.0 ± 0.8 g at 8 and 12 weeks, respectively (Fig. S5A). In addition, μ CT analysis was conducted to further examine cortical bone microarchitecture of *Lepr-cre;tdTomato;AC6^{fl/fl}* and *Lepr-cre;tdTomato* mice tibias. The total area, cortical area, cortical thickness, I_{\min} , and I_{\max} at the tibial midshaft of *Lepr-cre;tdTomato;AC6^{fl/fl}* mice were not significantly different from *Lepr-cre;tdTomato* mice (Fig. 5C). Collectively, these data indicate that there were no differences in the skeletal morphology of young-adult *Lepr-cre;tdTomato* and

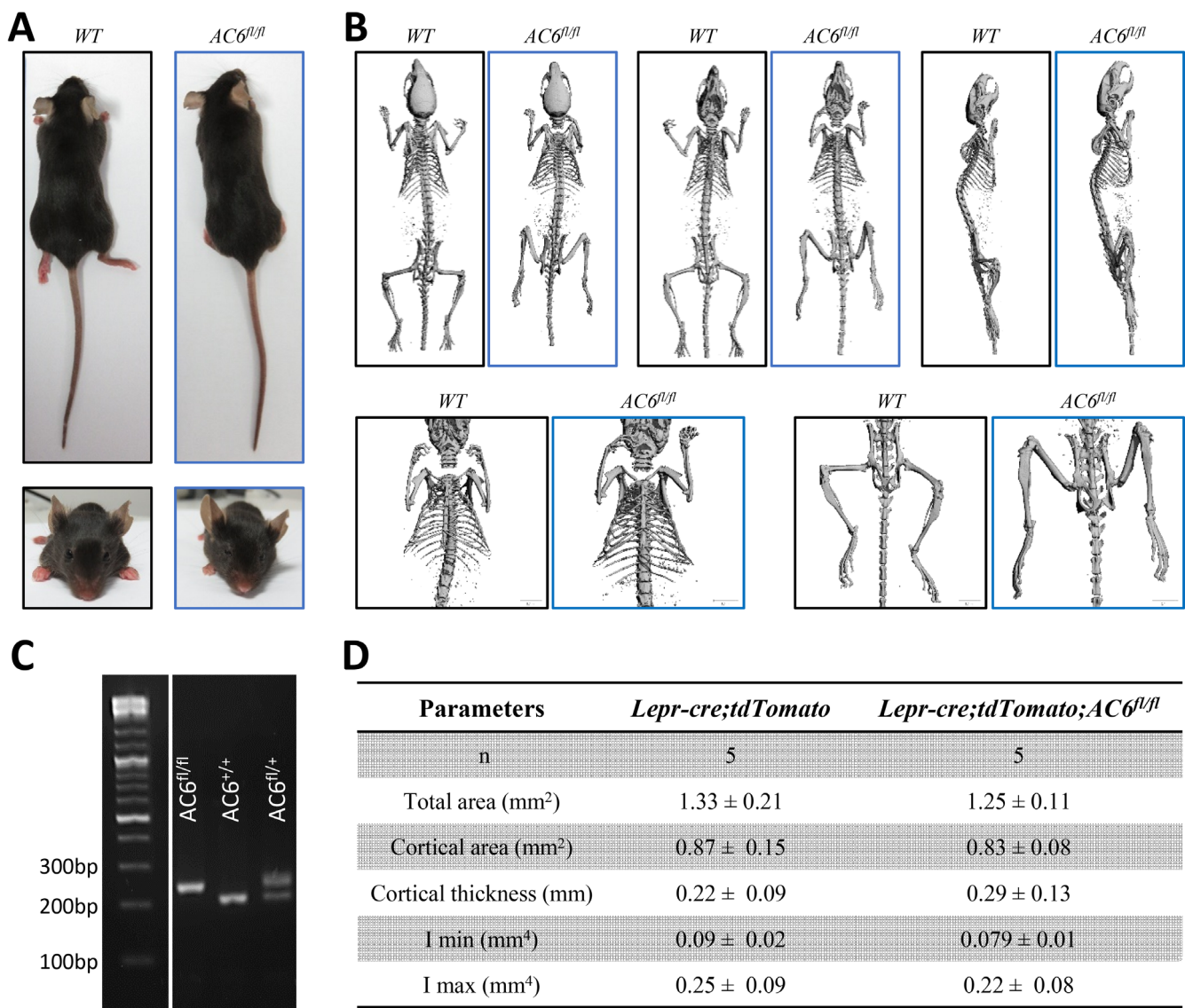


Fig 5. Phenotypic analysis of *Lepr-cre;tdTomato* and *Lepr-cre;tdTomato;AC6^{fl/fl}* mice at 8 and 12 weeks. (A) Photographs of *Lepr-cre;tdTomato* and *Lepr-cre;tdTomato;AC6^{fl/fl}* mice at 12 weeks old. (B) Full-body μ CT scans comparing the two genotypes. (C) Gel electrophoresis of genotyping showing a band at 260 bp for AC6 floxed gene. (D) Cortical bone midshaft geometry of 12-week-old *Lepr-cre;tdTomato* and *Lepr-cre;tdTomato;AC6^{fl/fl}* mice.

Lepr-cre;tdTomato;AC6^{fl/fl} mice. Thus, these results suggest *Lepr-cre;tdTomato;AC6^{fl/fl}* mice do not exhibit a gross morphological or skeletal phenotype, which is consistent with the *AC6* global deletion model.⁽²⁹⁾

As there is no skeletal phenotype following *AC6* deletion, an identical tibial-loading regime was applied to the *Lepr-cre;tdTomato;AC6^{fl/fl}* mice, and μ CT measurements were taken along the entire tibia length at the end of the loading period (Fig. 6A). Interestingly, no changes were observed for tibial cross-sectional area, ellipticity (Fig. 6A), thickness of the cortical bone, I_{\min} , I_{\max} or the resistance to torsion (Fig. S7) following the application of load in these *Lepr-cre;tdTomato;AC6^{fl/fl}* mice. This result shows that the deletion of *AC6* in a LepR-specific manner prevents the load-induced cortical bone formation otherwise observed.

Dynamic histomorphometry was utilized to further evaluate the effect of loading on cortical bone formation in *Lepr-cre;tdTomato;AC6^{fl/fl}* mice (Fig. 6B,C). No changes in mineralized surface, MAR, or BFR were found at the endosteal surface of tibial cortical bone in *Lepr-cre;tdTomato;AC6^{fl/fl}* postloading (Fig. 6B), which is in agreement with the μ CT analysis. However, on the periosteal surface, loading of *Lepr-cre;tdTomato;AC6^{fl/fl}* tibia resulted in an increase in mineralized surface and BFR, whereas no change in MAR was detected (Fig. 6C).

This effect of loading on *Tomato⁺;AC6^{-/-}* cells lining and embedded within bone was further assessed using histology (Fig. 7A). Mechanical loading did not change the percentage of *Tomato⁺;AC6^{-/-}* cells observed in any region of the tibia (Fig. 7B). The percentages of *Tomato⁺;AC6^{-/-}* cells on the endosteum, periosteum, and embedded within the cortical bone were investigated, and no effect of loading on cell number was evident. These data indicate that *Lepr-cre;tdTomato;AC6^{fl/fl}* animals have both an attenuated endosteal osteogenic response to loading and exhibit no change in the percentage of local *Lepr-cre;tdTomato⁺* cells. This, therefore, indicates that *LepR⁺* cells contribute to bone formation on the endosteal surface and that *AC6* is required in these cells to mediate this response.

Discussion

Bone marrow stromal/stem cells represent a quiescent cell population that supply bone-forming osteoblast cells to maintain tissue homeostasis and to facilitate repair in response to injury. A potent mediator of stromal/stem cell differentiation in vitro and bone formation in vivo is mechanical loading, yet it is unclear whether load-induced bone formation requires the recruitment and differentiation of resident progenitor cells. Therefore, in this study, we utilized the leptin receptor to identify and trace the contribution of bone marrow stromal cells and their progeny to bone mechanoadaptation. *Lepr-cre;tdTomato⁺* cells were tracked from E19.5 to early adulthood, to find that *Lepr-cre;tdTomato⁺* cells initially appear perivascularly within the marrow, perinatally, and increase in number with age, contributing to osteoblast and osteocyte populations signifying osteogenic lineage commitment. Compressive loading of *Lepr-cre;tdTomato* tibias resulted in increased bone formation on the endosteal and periosteal surface of cortical bone. Interestingly, no significant increase in the percentage of *Lepr-cre;tdTomato⁺* stromal cells within the bone marrow was observed, whereas no significant changes in the number of *Lepr-cre;tdTomato⁺* cells lining the bone surface or osteocytes embedded in bone were found following loading. *AC6* deletion in *Lepr-cre;tdTomato⁺* cells resulted in a reduced endocortical bone-forming response to loading, indicating a critical role for

Lepr-cre;tdTomato⁺ cell progeny in loading-induced bone formation. In summary, these data indicate that mechanical loading does not result in the proliferation of *Lepr-cre;tdTomato⁺* stromal cells within the marrow or in the recruitment of these cells to the bone surface, suggesting that these cells may play either a supportive role in osteogenesis via cell nonautonomous effects, or alternatively *LepR⁺* cells already present along the bone surface are reactivated, mediating short-term load-induced bone formation in a manner that is dependent on *AC6*.

The leptin receptor is expressed prenatally in bone and brain tissue and becomes widely expressed in nearly all major organs postnatally. Using confocal microscopy, the expression pattern of *Lepr-cre;tdTomato⁺* cells was analyzed in E19.5 mice. During this late stage of gestation, a limited number of *Lepr-cre;tdTomato⁺* cells were found to be present only in the brain and bone tissue. This is consistent with previous work that found no *Lepr-cre;tdTomato⁺* cells in the ossification center of bone at E15.5,⁽²⁰⁾ and limited *LepR*-positive cells at E19.5, indicating little contribution of these cells to bone formation at these earlier stages of development.⁽³⁾ The number of *Lepr-cre;tdTomato⁺* in the metaphyseal bone marrow showed a sharp increase by postnatal day P0.5,⁽³⁾ and in 1-week-old mice *LepR⁺* cells were present throughout the bone marrow.⁽²⁰⁾ Our data, in combination with previous work, suggest that *Lepr-cre;tdTomato⁺* cells increase in the bone marrow during bone maturation. We have also shown that *Lepr-cre;tdTomato⁺* cells were present within the brain at E19.5 and are found in the heart, lungs, spleen, liver, and the medulla region of the kidney in 8- and 12-week-old animals. Further interrogation by mRNA expression analysis of *LepR* in various mouse tissues also found that the heart and spleen have the lowest expression of *LepR* of the tissues analyzed,⁽²²⁾ which is consistent with our findings. This wide expression of leptin receptor has considerable implications for the use of the leptin receptor for the study of MSC behavior in bone, particularly when combined with Cre-lox strategy for gene deletion.

Within bone, *Lepr-cre;tdTomato⁺* cells appear perivascularly in the marrow, where they are recruited to the bone surface and commit to the osteogenic lineage with age. The percentage of *Lepr-cre;tdTomato⁺* cells within the tibial marrow increased between 8 and 12 weeks of age, suggesting a maturation-related expansion of this cell type. This increase in marrow *Lepr-cre;tdTomato⁺* cells was mirrored by an increase in *tdTomato⁺* cells on both bone surfaces and embedded with bone. Similar findings were reported by Zhou and colleagues, where the percentage of *Lepr-cre;tdTomato⁺* cells making up *Col2.3-GFP⁺* osteoblast cells increased from 10% to 81% from 6 to 14 months of age.⁽³⁾ This earlier study also found that the increase was not caused by the induced expression of *LepR* at this age, but rather by the proliferation and differentiation of *LepR* cells resident in the bone marrow.⁽³⁾ Furthermore, we did not observe *LepR* immunolabeling in cells located on the bone surface or embedded in the bone matrix in our *Lepr-cre;tdTomato* mice, and studies at 15 weeks in the same mouse model have shown that *tdTomato⁺* cells in the bone tissue were osteocalcin- and dentin matrix protein-1- (*DMP1*-) expressing mature osteoblasts and osteocytes, respectively.⁽²⁰⁾ Importantly, *LepR* mRNA was not detectable by quantitative real-time PCR in the osteoblasts, suggesting that *Lepr-cre;tdTomato⁺* mature bone cells do not autonomously express *LepR*, but are descendants of *LepR⁺* precursors.⁽²⁰⁾ Taken together, these data show that the leptin receptor is a robust marker of MSCs in vivo to trace their progeny.

Although the contribution of *Lepr-cre;tdTomato⁺* cells to adult bone formation has been investigated, their contribution

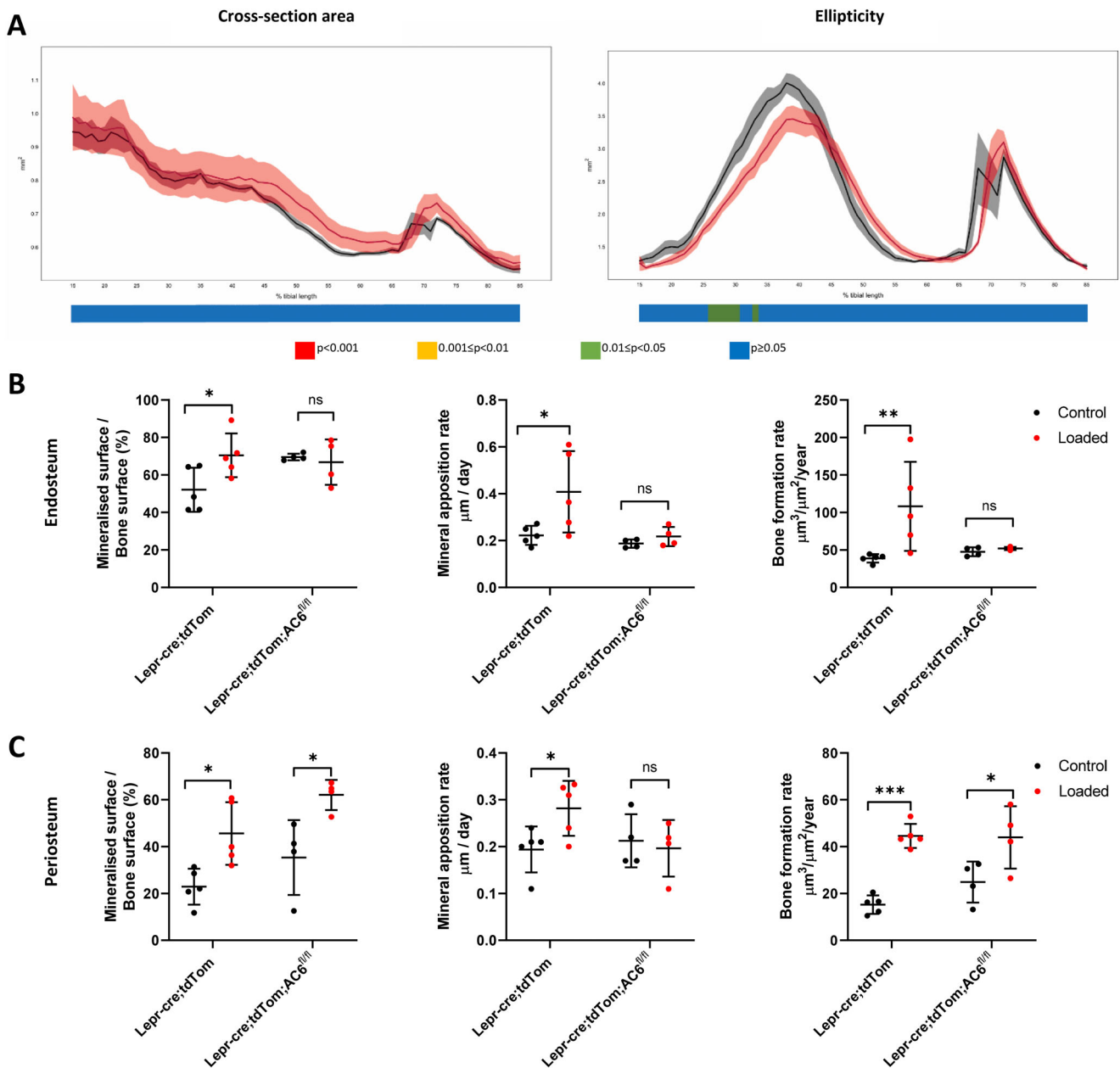


Fig 6. Axial tibia loading of 12-week-old *Lepr-cre;tdTomato;AC6^{fl/fl}* mice. (A) Whole-bone analyses of cortical bone of mice lacking AC6 between 15% and 85% of the total tibial length, excluding proximal and distal metaphyseal bone showing cross-sectional area and ellipticity. Loaded: red, static: black, line graphs represent means \pm SEM, $n = 6$. Statistical significance of differences along the entire tibial shaft is represented as a heat map, red $p < 0.001$, yellow $0.001 \leq p < 0.01$, green $0.01 \leq p < 0.05$, and blue $p \geq 0.05$. (B,C) Mice lacking AC6 showed poor mineralization on the endosteal surface, indicated by a lack of labeling at the endosteal surface in both loaded and nonloaded tibias. (B) Relative mineralizing surface over bone surface, mineral apposition rate, and bone formation rate at the endosteal surface of mechanically loaded tibia. (C) Relative mineralizing surface over bone surface, mineral apposition rate, and bone formation rate at the periosteal surface. $N = 5$ for *Lepr-cre;tdTomato*. $N = 3$ for *Lepr-cre;tdTomato;AC6^{fl/fl}*. Mean \pm SD.

to load-induced bone formation has not been examined to date. Herein, in vivo mechanical loading of *Lepr-cre;tdTomato* mouse tibia resulted in no change in the percentage of *Lepr-cre;tdTomato*⁺ cells along the bone surface or osteocytes, suggesting that this loading protocol does not initiate recruitment of *Lepr-cre;tdTomato*⁺ marrow cells, but instead activates resident cells at the bone surface. This is in close agreement with several previous observations made in other models of bone loading, where early-loading-related activation of osteoblast metabolic activity

was observed and where there was evidence for the direct transformation from quiescence to bone formation in the adult periosteum following a single brief period of bone loading.^(35,36)

The loading protocol used in this study spanned 2 weeks; therefore, although loading induced a trend in an increase in the percentage of *Lepr-cre;tdTomato*⁺ marrow stromal cells, these *Lepr*⁺ progenitor cells did not contribute to bone formation within the time frame studied. Recent work from Yang and colleagues also found a lack of response in this cell population

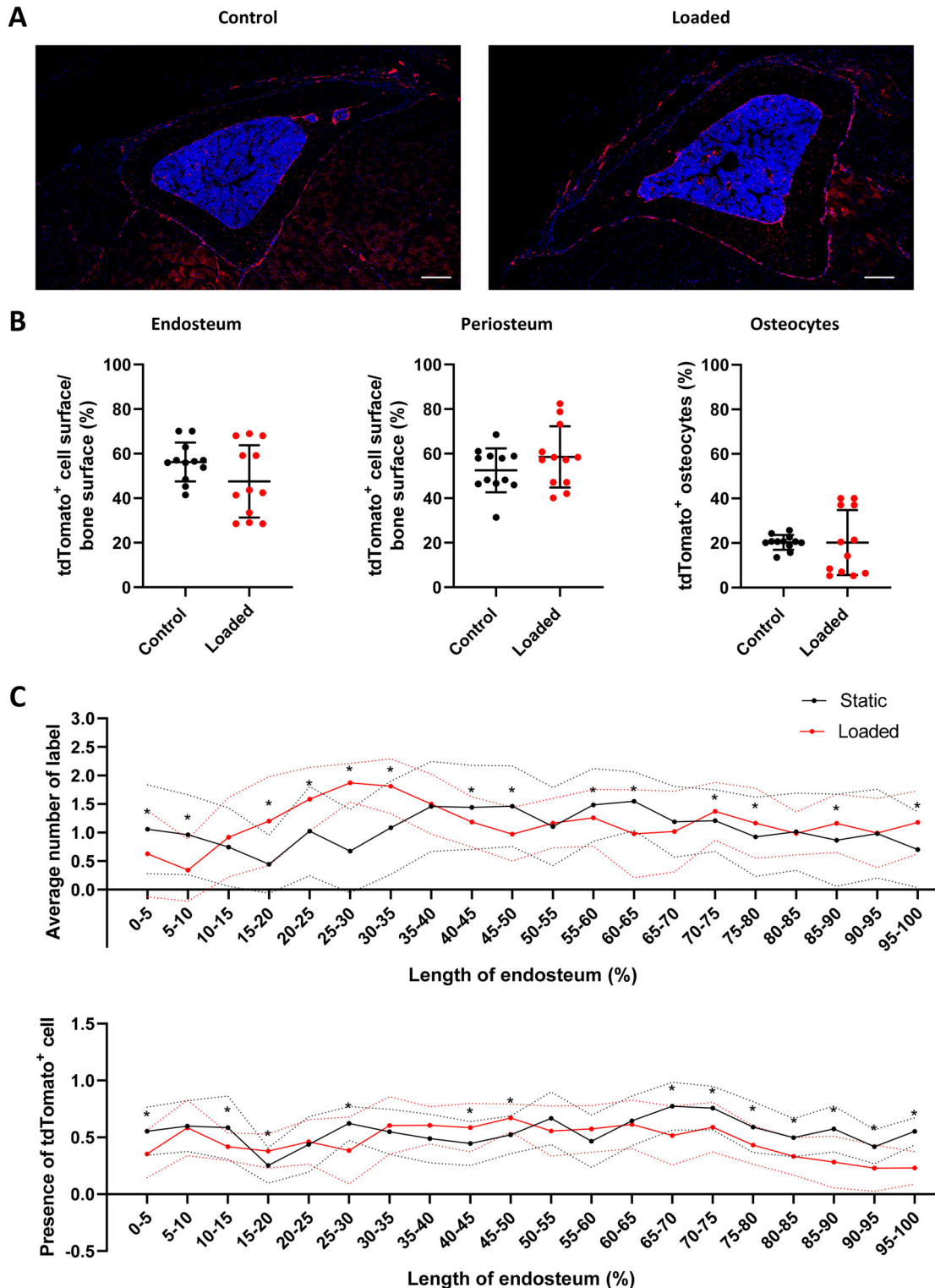


Fig 7. Tibial compressive loading does not alter proliferation or location of *Lepr-cre;tdTomato* cells in *Lepr-cre;tdTomato* and *Lepr-cre;tdTomato;AC6^{fl/fl}* mice. (A) Representative image of tibia transection of *Lepr-cre;tdTomato;AC6^{fl/fl}* mice following tibia compressive loading; scale bar = 100 μ m. (B) The percentage of tdTomato⁺ cells on the endosteal and periosteal surfaces and embedded with the bone was not altered in cortical bone; $N = 4$. Statistical tests employed unpaired two-tailed student *t* test with Wilcoxon correction. Mean \pm SD. (C) Analysis of the location of bone formation along the surface of the endosteum. Upper graph: Average number of label observed by dynamic histomorphometry; $n = 4$. Lower graph: Average number of tdTomato⁺ cells observed lining endosteum surface on confocal images; $n = 3$. Statistical tests employed unpaired two-tailed student *t* test. Mean \pm SD; * $p < 0.05$.

following 10 days of iPTH treatment in the femoral marrow.⁽¹⁸⁾ Interestingly, this finding of reactivation of mature cells is consistent with a study by Chow and colleagues, where loading of the caudal vertebra resulted in reactivation of previously quiescent bone-lining cells.⁽³⁷⁾ As with the present study, the rapidity with which new bone was formed following mechanical stimulation raised the potential for this bone formation to occur via the reactivation of cells already along the bone surface, rather than recruitment from the stem cell niche. Recently, Matic and colleagues observed labeled bone surface cells at time points extending beyond the reported lifespan for an osteoblast, suggesting that continuous reactivation of bone-lining cells is a potential mechanism of adult bone adaptation.⁽³⁸⁾ Other recent studies have reported proliferation of osteoprogenitor Prrx1⁺-Sca1⁺ cells⁽⁷⁾ and preosteoblast Osx⁺ cells⁽²³⁾ as a major contributor to loading-induced bone formation and not the differentiation of stem cells, which further strengthens our findings.

The specific knockout of AC6 in LepR⁺ cells does not induce a skeletal phenotype, but results in abolition of load-induced adaptive responses at the endocortical surface, providing a critical role for LepR⁺ cells and their progeny in bone mechanoadaptation. The absence of a basal skeletal phenotype in *Lepr-cre;tdTomato;AC6^{fl/fl}* mice suggests that AC6 does not play a role in skeletal development. However, the disruption of bone mechanoadaptation on the endosteal surface in *Lepr-cre;tdTomato;AC6^{fl/fl}* mice proves the importance of AC6 in load-induced bone formation. At the time of loading, approximately 50% of the bone surface is covered by cells derived from LepR⁺ cells; these cells may be responsible for the anabolic bone response—this is consistent with our in vitro studies highlighting a vital role for AC6 in MSC and mature bone cell mechanotransduction.^(25,29) However, we cannot yet directly rule out the possibility that LepR⁺ cells in the marrow may contribute to the activation of non-*Lepr-cre;tdTomato⁺* cells on the bone surface in a nonautonomous manner.

Although the response on the periosteal surface was blunted, the bone-forming response observed at this location may be attributed to other non-LepR⁺ cells potentially recruited from the periosteum.⁽³⁹⁾ For example, Duchamp de Lageneste and colleagues described a population of skeletal stem cells labeled by Prrx1⁺ in the periosteum that expressed markers shown to define mouse skeletal stem cells, but were negative for leptin receptor.⁽³⁹⁾ Moreover, it was shown by Moore and colleagues that Prrx1⁺ cells resident in the periosteum can sense and respond to physical stimulation in vivo and contribute to the load-induced bone formation.⁽⁴⁰⁾ Additional work is required to draw conclusive findings; however, in our experiment this LepR⁻/Prrx1⁺ cell population would not have been targeted by the AC6 deletion, and thus may play a role in the load-induced bone-forming response observed on the periosteal surface.

This diminished mechanoadaptive response is in agreement with work examining a global knockout of AC6, where AC6 deletion resulted in an inhibited response to ulna loading,⁽²⁹⁾ and further strengthens the potential involvement of the primary cilium, to which AC6 localizes, in bone mechanoadaptation.^(41,42) Furthermore, as with the *Lepr-cre;tdTomato* mouse, no change was found in the percentage of *Lepr-cre;tdTomato⁺* cells on the bone surface or embedded within the bone. The lack of bone formation and the failure of loading to induce migration of LepR⁺ cells from the marrow to the bone surface in *Lepr-cre;tdTomato;AC6^{fl/fl}* mice are consistent with our hypothesis that loading-induced bone formation occurs via *Lepr-cre;tdTomato⁺* cells, and that this process requires AC6.

Conclusions

In conclusion, this study has characterized the contribution of LepR⁺ bone marrow stromal cells to bone formation during growth and in response to mechanical loading. Interestingly, although LepR⁺ stromal cells are the main source of osteoblasts and osteocytes with age, they are not recruited to the bone surface in response to short-term loading. Rather, LepR⁺ cells contribute to bone formation either through a supportive role via cell nonautonomous effects, or alternatively, LepR⁺ cells already present along the bone surface are reactivated. Interestingly, this activation requires AC6, which has previously been shown to be an important component of stem cell and mature bone cell mechanotransduction.

Disclosures

The authors have no conflicts of interest.

Acknowledgments

This publication emanated from research conducted with the financial support of Science Foundation Ireland (SFI) and is cofunded under the European Regional Development Fund under an AMBER award (Grant No. 12/RC/2278_2). The authors acknowledge funding from the Irish Research Council Government of Ireland Postgraduate Scholarship (Grant No. GOIPG/2014/1463), the European Research Council (ERC; Starting Grant No. 336882), the SFI (Support Grant SFI 13/ERC/L2864), the Biotechnology and Biological Sciences Research Council (Grant No. BB/I014608/1), and Arthritis Research UK (Grant No. 20581). Flow cytometry was performed in the TCD Flow Cytometry Facility, funded by the Irish Higher Education Authority Programme for Research in Third Level Institute and Science Foundation Ireland [Grant No. 12/RI/2340(7)].

Authors' roles: DAH was responsible for the experimental concept and objectives. MR, GPJ, and DAH designed the experiments. GPJ and MR performed the experiments and collected the data. GPJ, MR, MMO, and BJ analyzed the data. GPJ, MR, BJ, AAP, and DAH interpreted the data. Approving final version of manuscript: MR, GPJ, MMP, BJ, AAP, and DAH.

Author Contributions

Mathieu Riffault: Conceptualization; data curation; formal analysis; investigation; methodology; validation; writing-original draft; writing-review and editing. **Gillian Johnson:** Conceptualization; data curation; formal analysis; funding acquisition; investigation; methodology; validation; visualization; writing-original draft; writing-review and editing. **Madeline Owen:** Data curation; formal analysis. **Behzad Javaheri:** Formal analysis; investigation; methodology; software; validation; writing-original draft; writing-review and editing. **Andrew Pitsillides:** Formal analysis; funding acquisition; investigation; methodology; supervision; validation; writing-original draft; writing-review and editing.

Peer Review

The peer review history for this article is available at <https://publons.com/publon/10.1002/jbm4.10408>.

References

1. Frost HM. Skeletal structural adaptations to mechanical usage (SATMU): 1. Redefining Wolff's law: the bone modeling problem. *Anat Rec*. 1990;226(4):403–13.
2. Meakin LB, Price JS, Lanyon LE. The contribution of experimental in vivo models to understanding the mechanisms of adaptation to mechanical loading in bone. *Front Endocrinol*. 2014;5:154.
3. Zhou BO, Yue R, Murphy MM, Peyer JG, Morrison SJ. Leptin-receptor-expressing mesenchymal stromal cells represent the main source of bone formed by adult bone marrow. *Cell Stem Cell*. 2014;15(2):154–68.
4. Park D, Spencer JA, Koh BI, et al. Endogenous bone marrow MSCs are dynamic, fate-restricted participants in bone maintenance and regeneration. *Cell Stem Cell*. 2012;10(3):259–72.
5. Stavenschi E, Labour MN, Hoey DA. Oscillatory fluid flow induces the osteogenic lineage commitment of mesenchymal stem cells: the effect of shear stress magnitude, frequency and duration. *J Biomech*. 2017;55:99–106.
6. Knight MN, Hankenson KB. Mesenchymal stem cells in bone regeneration. *Adv Wound Care*. 2016;2(6):306–16.
7. Liu C, Cabahug-Zuckerman P, Stubbs C, et al. Mechanical loading promotes the expansion of primitive Osteoprogenitors and organizes matrix and vascular morphology in long bone defects. *J Bone Miner Res*. 2019;34(5):896–910.
8. Brady RT, O'Brien FJ, Hoey DA. Mechanically stimulated bone cells secrete paracrine factors that regulate osteoprogenitor recruitment, proliferation, and differentiation. *Biochem Biophys Res Commun*. 2015;459(1):118–23.
9. Curtis KJ, Coughlin TR, Mason DE, Boerckel JD, Niebur GL. Bone marrow mechanotransduction in porcine explants alters kinase activation and enhances trabecular bone formation in the absence of osteocyte signaling. *Bone*. 2018;107:78–87.
10. Stavenschi E, Corrigan MA, Johnson GP, Riffault M, Hoey DA. Physiological cyclic hydrostatic pressure induces osteogenic lineage commitment of human bone marrow stem cells: a systematic study. *Stem Cell Res Ther*. 2018;9(1):276.
11. Bianco P, Robey PG, Simmons PJ. Mesenchymal stem cells: revisiting history, concepts, and assays. *Cell Stem Cell*. 2008;2(4):313–9.
12. Morikawa S, Mabuchi Y, Kubota Y, et al. Prospective identification, isolation, and systemic transplantation of multipotent mesenchymal stem cells in murine bone marrow. *J Exp Med*. 2009;206(11):2483–96.
13. Nakao N, Nakayama T, Yahata T, et al. Adipose tissue-derived mesenchymal stem cells facilitate hematopoiesis in vitro and in vivo: advantages over bone marrow-derived mesenchymal stem cells. *Am J Pathol*. 2010;177(2):547–54.
14. Chan CK, Seo EY, Chen JY, Lo D, McArdle A. Sinha, et al. Identification and specification of the mouse skeletal stem cell. *Cell*. 2015;160(1–2):285–98.
15. Ding L, Saunders TL, Enikolopov G, Morrison SJ. Endothelial and perivascular cells maintain haematopoietic stem cells. *Nature*. 2012;481(7382):457–62.
16. Ding L, Morrison SJ. Haematopoietic stem cells and early lymphoid progenitors occupy distinct bone marrow niches. *Nature*. 2013;495(7440):231–5.
17. Caire R, Roche B, Picot T, et al. Parathyroid hormone remodels bone transitional vessels and the Leptin receptor-positive Pericyte network in mice. *J Bone Miner Res*. 2019;34(8):1487–501.
18. Yang M, Arai A, Udagawa N, et al. Parathyroid hormone shifts cell fate of a Leptin receptor-marked stromal population from Adipogenic to Osteoblastic lineage. *J Bone Miner Res*. 2019;34(10):1952–63.
19. Tikhonova AN, Dolgalev I, Hu H, et al. The bone marrow microenvironment at single-cell resolution. *Nature*. 2019;569(7755):222–8.
20. Mizoguchi T, Pinho S, Ahmed J, et al. Osterix marks distinct waves of primitive and definitive stromal progenitors during bone marrow development. *Dev Cell*. 2014;29(3):340–9.
21. DeFalco J, Tomishima M, Liu H, et al. Virus-assisted mapping of neural inputs to a feeding center in the hypothalamus. *Science*. 2001;291(5513):2608–13.
22. Fei H, Okano HJ, Li C, et al. Anatomic localization of alternatively spliced leptin receptors (Ob-R) in mouse brain and other tissues. *Proc Natl Acad Sci U S A*. 1997;94(13):7001–5.
23. Zannit HM, Silva MJ. Proliferation and activation of Osterix-lineage cells contribute to loading-induced periosteal bone formation in mice. *JBMR Plus*. 2019;3(11):e10227.
24. Stavenschi E, Labour MN, Hoey DA. Oscillatory fluid flow induces the osteogenic lineage commitment of mesenchymal stem cells: the effect of shear stress magnitude, frequency, and duration. *J Biomech*. 2017;55:99–106.
25. Johnson GP, Stavenschi E, Eichholz KF, Corrigan MA, Fair S, Hoey DA. Mesenchymal stem cell mechanotransduction is cAMP dependent and regulated by adenylyl cyclase 6 and the primary cilium. *J Cell Sci*. 2018;131(21):jcs.222737.
26. Kamenetsky M, Middelhaufe S, Bank EM, Levin LR, Buck J, Steegborn C. Molecular details of cAMP generation in mammalian cells: a tale of two systems. *J Mol Biol*. 2006;362(4):623–39.
27. Hanoune J, Defer N. Regulation and role of adenylyl cyclase isoforms. *Annu Rev Pharmacol Toxicol*. 2001;41:145–74.
28. Defer N, Best-Belpomme M, Hanoune J. Tissue specificity and physiological relevance of various isoforms of adenylyl cyclase. *Am J Physiol Renal Physiol*. 2000;279(3):F400–16.
29. Lee KL, Hoey DA, Spasic M, Tang T, Hammond HK, Jacobs CR. Adenylyl cyclase 6 mediates loading-induced bone adaptation in vivo. *FASEB J*. 2014;28(3):1157–65.
30. Madisen L, Zwingman TA, Sunkin SM, et al. A robust and high-throughput Cre reporting and characterization system for the whole mouse brain. *Nat Neurosci*. 2010;13(1):133–40.
31. Roos KP, Strait KA, Raphael KL, Blount MA, Kohan DE. Collecting duct-specific knockout of adenylyl cyclase type VI causes a urinary concentration defect in mice. *Am J Physiol Renal Physiol*. 2012;302(1):F78–84.
32. De Souza RL, Matsuura M, Eckstein F, Rawlinson SC, Lanyon LE, Pittsillides AA. Non-invasive axial loading of mouse tibiae increases cortical bone formation and modifies trabecular organization: a new model to study cortical and cancellous compartments in a single loaded element. *Bone*. 2005;37(6):810–8.
33. Doube M, Klosowski MM, Arganda-Carreras I, et al. BoneJ: free and extensible bone image analysis in ImageJ. *Bone*. 2010;47(6):1076–9.
34. Schindelin J, Arganda-Carreras I, Frise E, et al. Fiji: an open-source platform for biological-image analysis. *Nat Methods*. 2012;9(7):676–82.
35. Dodds RA, Ali N, Pead MJ, Lanyon LE. Early loading-related changes in the activity of glucose 6-phosphate dehydrogenase and alkaline phosphatase in osteocytes and periosteal osteoblasts in rat fibulae in vivo. *J Bone Miner Res*. 1993;8(3):261–7.
36. Pead MJ, Skerry TM, Lanyon LE. Direct transformation from quiescence to bone formation in the adult periosteum following a single brief period of bone loading. *J Bone Miner Res*. 1988;3(6):647–56.
37. Chow JW, Wilson AJ, Chambers TJ, Fox SW. Mechanical loading stimulates bone formation by reactivation of bone lining cells in 13-week-old rats. *J Bone Miner Res*. 1993;13(11):1760–7.
38. Matic I, Matthews BG, Wang X, et al. Quiescent bone lining cells are a major source of osteoblasts during adulthood. *Stem Cells*. 2016;34(12):2930–42.
39. Duchamp de Lageneste O, Julien A, Abou-Khalil R, et al. Periosteum contains skeletal stem cells with high bone regenerative potential controlled by periostin. *Nat Commun*. 2018;9(1):773.
40. Moore ER, Yang Y, Jacobs CR. Primary cilia are necessary for Prx1-expressing cells to contribute to postnatal skeletogenesis. *J Cell Sci*. 2018;131(16):jcs.217828.
41. Moore ER, Chen JC, Jacobs CR. Prx1-expressing progenitor primary cilia mediate bone formation in response to mechanical loading in mice. *Stem Cells Int*. 2019;2019:3094154.
42. Chen JC, Hoey DA, Chua M, Bellon R, Jacobs CR. Mechanical signals promote osteogenic fate through a primary cilia-mediated mechanism. *FASEB J*. 2016;30(4):1504–11.